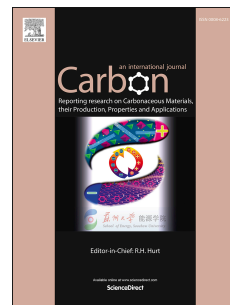


Accepted Manuscript

Measured *in-situ* mass absorption spectra for nine forms of highly-absorbing carbonaceous aerosol

Christopher D. Zangmeister, Rian You, Elizabeth M. Lunny, Arne E. Jacobson, Mitchio Okumura, Michael R. Zachariah, James G. Radney



PII: S0008-6223(18)30418-4

DOI: [10.1016/j.carbon.2018.04.057](https://doi.org/10.1016/j.carbon.2018.04.057)

Reference: CARBON 13094

To appear in: *Carbon*

Received Date: 8 December 2017

Revised Date: 19 April 2018

Accepted Date: 21 April 2018

Please cite this article as: C.D. Zangmeister, R. You, E.M. Lunny, A.E. Jacobson, M. Okumura, M.R. Zachariah, J.G. Radney, Measured *in-situ* mass absorption spectra for nine forms of highly-absorbing carbonaceous aerosol, *Carbon* (2018), doi: 10.1016/j.carbon.2018.04.057.

This is a PDF file of an unedited manuscript that has been accepted for publication. As a service to our customers we are providing this early version of the manuscript. The manuscript will undergo copyediting, typesetting, and review of the resulting proof before it is published in its final form. Please note that during the production process errors may be discovered which could affect the content, and all legal disclaimers that apply to the journal pertain.

Measured *In-situ* Mass Absorption Spectra for Nine Forms of Highly-absorbing Carbonaceous Aerosol

Christopher D. Zangmeister^{a,*}, Rian You^{a,b}, Elizabeth M. Lunny^c, Arne E. Jacobson^d, Mitchio Okumura^c, Michael R. Zachariah^{a,b}, and James G. Radney^a

^a Material Measurement Laboratory, National Institute of Standards and Technology, Gaithersburg, MD 20899

^b Department of Chemistry and Biochemistry, University of Maryland College Park, College Park, MD 20742

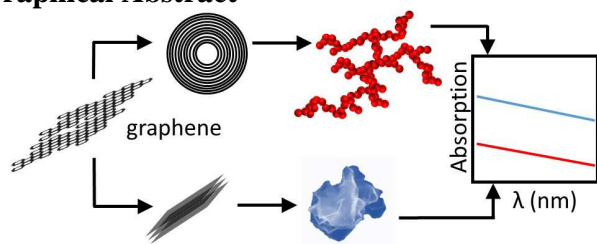
^c Division of Chemistry and Chemical Engineering, California Institute of Technology, Pasadena, California, 91125

^d Environmental Resources Engineering, Humboldt State University, Arcata, California, 95521

Abstract

Mass absorption coefficient spectra were measured between $\lambda = 500$ nm and 840 nm for nine forms of highly-absorbing carbonaceous aerosol: five samples generated from gas-, liquid- and solid-fueled flames; spark-discharge fullerene soot; graphene and reduced graphene oxide (rGO) crumpled nanosheets; and fullerene (C_{60}) assemblies. Aerosol absorption spectra were measured for size- and mass-selected particles and found to be dependent on fuel type and formative conditions. Flame-generated particles had morphologies consistent with freshly emitted black carbon (BC) with mass absorption coefficients (MAC) ranging between $3.8 \text{ m}^2 \text{ g}^{-1}$ and $8.6 \text{ m}^2 \text{ g}^{-1}$ at $\lambda = 550$ nm. Absorption Ångström exponents (AAE) – i.e. MAC spectral dependence – ranged between 1.0 and 1.3 for flame-generated particles and up to 7.5 for C_{60} . The dependence of MAC and AAE on mobility diameter and particle morphology was also investigated. Lastly, the current data were compared to all previously published MAC measurements of highly-absorbing carbonaceous aerosol.

Graphical Abstract



1 Measured *In-situ* Mass Absorption Spectra for Nine 2 Forms of Highly-absorbing Carbonaceous Aerosol

3 Christopher D. Zangmeister^{a,*}, Rian You^{a,b}, Elizabeth M. Lunny^c, Arne E. Jacobson^d, Mitchio
4 Okumura^c, Michael R. Zachariah^{a,b}, and James G. Radney^a

5 ^a Material Measurement Laboratory, National Institute of Standards and Technology,
6 Gaithersburg, MD 20899

7 ^b Department of Chemistry and Biochemistry, University of Maryland College Park, College
8 Park, MD 20742

9 ^c Division of Chemistry and Chemical Engineering, California Institute of Technology,
10 Pasadena, California, 91125

11 ^d Environmental Resources Engineering, Humboldt State University, Arcata, California, 95521

12 **Abstract**

13 Mass absorption coefficient spectra were measured between $\lambda = 500$ nm and 840 nm for nine
14 forms of highly-absorbing carbonaceous aerosol: five samples generated from gas-, liquid- and
15 solid-fueled flames; spark-discharge fullerene soot; graphene and reduced graphene oxide (rGO)
16 crumpled nanosheets; and fullerene (C₆₀) assemblies. Aerosol absorption spectra were measured
17 for size- and mass-selected particles and found to be dependent on fuel type and formative
18 conditions. Flame-generated particles had morphologies consistent with freshly emitted black
19 carbon (BC) with mass absorption coefficients (*MAC*) ranging between 3.8 m² g⁻¹ and 8.6 m² g⁻¹
20 at $\lambda = 550$ nm. Absorption Ångström exponents (*AAE*) – i.e. *MAC* spectral dependence – ranged
21 between 1.0 and 1.3 for flame-generated particles and up to 7.5 for C₆₀. The dependence of *MAC*
22 and *AAE* on mobility diameter and particle morphology was also investigated. Lastly, the current

* Corresponding Author. E-mail: cdzang@nist.gov. Phone: (301)975-8709. Fax: (301)975-3670

¹ These authors contributed equally to this work.

All authors have given approval of the final version of the manuscript.

23 data were compared to all previously published *MAC* measurements of highly-absorbing
24 carbonaceous aerosol.

25 1. Introduction

26 Highly-absorbing carbonaceous aerosol forms during the incomplete combustion of carbon-
27 containing fuels. Due to the diversity of matter in the atmosphere, black carbon aerosol (BC) has
28 been delineated from other suspended carbonaceous nanomaterials and narrowly defined by its
29 chemical, physical and spectroscopic properties. BC is composed of nearly-elemental carbon
30 with extended sp^2 -bonding between carbon atoms arranged in multi-layered graphene-like sheets
31 forming concentric, spherical nanoscale monomers aggregated into an open, lacey structure [1,
32 2], see Figure 1. The lacey aggregates may rearrange (collapse) into a compact, spherical, void-
33 filled morphology after interaction with condensed- and/or gas-phase species [3-5]. Other similar
34 carbonaceous nanomaterials can form under different conditions impacting the material's
35 physical and, potentially, spectroscopic properties. For example, graphene and reduced graphene
36 oxide (rGO) form crumpled nanopaper-like structures [6-9], see Figure 1, chemically analogous
37 to BC but morphologically dissimilar. It is unclear how, or if, these properties impact light
38 absorption.

39 BC is spectroscopically defined as a material with a mass-specific (mass-normalized)
40 absorption cross-section of $7.5 \pm 1.2 \text{ m}^2 \text{ g}^{-1}$ at $\lambda = 550 \text{ nm}$, the solar transmission maximum [1].
41 From the Beer-Lambert Law, the absorption coefficient ($\alpha_{abs}, \text{m}^{-1}$) is the product of the number
42 density of absorbers (N, m^{-3}) and their corresponding absorption cross-sections (C_{abs}, m^2)

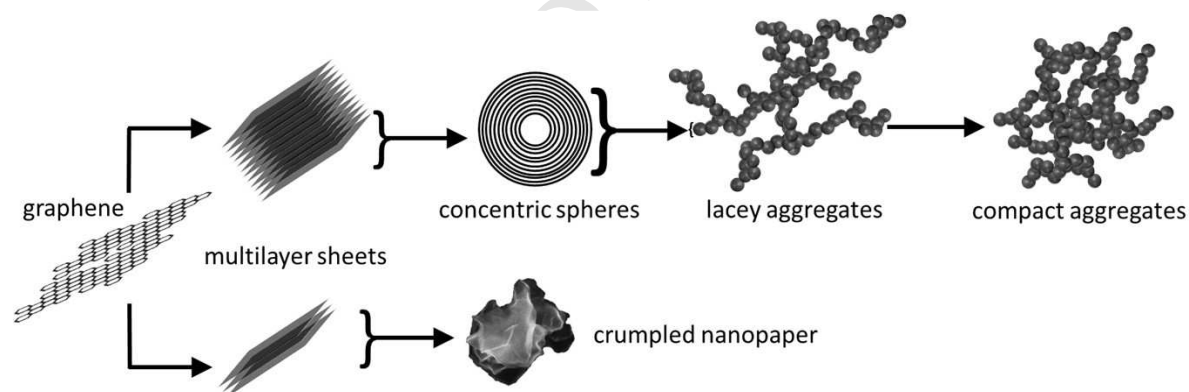
$$43 \alpha_{abs} = N * C_{abs} = N * m_p * MAC = M * MAC \quad (1)$$

44 If particle mass (m_p, g), or the ensemble mass concentration ($M, \text{g m}^{-3}$) is known, it is possible to
45 parameterize α_{abs} in terms of *MAC* ($\text{m}^2 \text{ g}^{-1}$). In the small particle (i.e. Rayleigh regime) or

46 optically-thin limits where absorption scales directly with mass (volume) [10, 11], MAC
 47 represents the mass-specific absorption cross-section. Otherwise, MAC represents the mass
 48 absorption coefficient; in some studies, the mass absorption efficiency (MAE) is also used [12-
 49 15]. In comparison to solution-phase spectroscopy, the mass-specific absorption cross-section
 50 and the mass absorption coefficient approximate the linear and non-linear regimes in absorption
 51 as a function of absorber number density (e.g. dilute and high concentration limits), respectively.
 52 For the remainder of this manuscript, MAC is used to refer to the mass absorption coefficient as
 53 the measured values of highly-absorbing carbonaceous particles may be size (mass) dependent
 54 (see Figure 5a and corresponding discussion). The wavelength dependence of MAC can be
 55 described by the absorption Ångström exponent (AAE)

$$56 \quad MAC_{\lambda} = MAC_{\lambda_0} \left(\frac{\lambda}{\lambda_0} \right)^{-AAE} \quad (2)$$

57 where λ and λ_0 are an arbitrary wavelength and a reference wavelength, respectively [16, 17].



58 **Figure 1.** Schematic of formation for graphene-based highly-absorbing carbonaceous
 59 nanomaterials. Top shows graphene-like sheets stacking and forming nanoscale concentric
 60 spheres that aggregate into lacey structures resembling freshly formed BC. Aggregates may
 61 become compacted upon interaction with gaseous or condensed phase materials. Bottom shows
 62 graphene-like material in single or multilayer sheets forming a nanoscale crumpled-paper
 63 morphology.
 64

65
 66 BC exhibits the second largest direct positive radiative forcing after CO_2 [1, 18, 19].

67 Quantitative assessment of an aerosol's radiative forcing requires its spectroscopic properties to

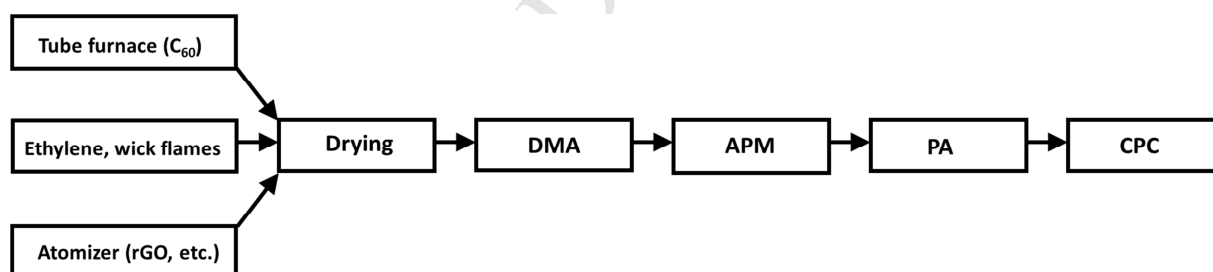
68 be well-known with minimal uncertainty across the ultraviolet to near-IR. The most
69 comprehensive assessments of highly-absorbing carbonaceous aerosols were reviews by Bond
70 and Bergstrom (2006) [1] and Bond, et al. (2013) [18] which focused on determination of BC
71 *MAC* using data from peer-reviewed publications. The previously published data were corrected
72 to account for presumed measurement biases and normalized to $\lambda = 550$ nm assuming an *AAE* of
73 1 (λ^{-1}); i.e. particles in the Rayleigh regime with a wavelength independent complex refractive
74 index ($m = n + ik$) over the desired wavelength interval [10, 11]. The studies used by Bond and
75 Bergstrom (2006) [1] reported a BC *MAC* ranging from $1.6 \text{ m}^2 \text{ g}^{-1}$ to $15.9 \text{ m}^2 \text{ g}^{-1}$ with an average
76 of $7.5 \pm 1.2 \text{ m}^2 \text{ g}^{-1}$ (1σ) at $\lambda = 550$ nm. Notably, none of the studies used in the assessments
77 directly measured *MAC* due to a lack, at the time, of reliable methods to measure aerosol mass
78 *in-situ*. In addition to the determination of radiative forcing from BC, measured *in-situ* spectral
79 properties, such as aerosol absorption and *AAE*, have also been used for aerosol identification
80 and source apportionment [20, 21].

81 The most direct method of obtaining *MAC* is to measure all experimental parameters: e.g.
82 ensemble absorption coefficients and average particle mass and number density, ensemble
83 absorption coefficients and mass concentration or single-particle absorption cross-section and
84 mass. Aerosol metrology, such as mass selectivity and *in-situ* spectroscopies, has improved
85 significantly since the 2006 BC *MAC* assessment enabling re-assessment. Newly developed
86 techniques have highlighted the need for inter-comparability of laboratory methods and the
87 development of aerosolizable materials for standards [22, 23]. This investigation explores
88 particle absorption for size- and mass-selected highly-absorbing carbonaceous aerosol. The goal
89 is to establish the range of mass-normalized aerosol absorption for this important class of
90 atmospherically relevant materials under controlled conditions and compare these data to other

91 studies. *MAC* of nine types of highly-absorbing carbonaceous aerosol was determined from
 92 measurements of α_{abs} , m_p and N using a photoacoustic spectrometer coupled to a broad-
 93 bandwidth ($\lambda = 500$ nm to 840 nm) light source, an aerosol particle mass analyzer and a
 94 condensation particle counter, respectively. Particles were generated from multiple sources to
 95 understand how aerosol formation conditions and material properties impact absorption. These
 96 data were compared to over four decades of published absorption data to aid in bounding the
 97 range of *MAC* measurements for this family of carbonaceous particles.

98 2. Materials and methods

99 A general experimental schematic is shown in Figure 2. Aerosol generation was specific for
 100 each sample and is described below. Aerosol was dried and mobility- and mass-classified using a
 101 differential mobility analyzer (DMA) and an aerosol particle mass analyzer (APM), respectively,
 102 prior to measurements of absorption coefficients and number concentration using a
 103 photoacoustic spectrometer (PA) and condensation particle counter (CPC), respectively.



104
 105
 106 **Figure 2.** Experimental schematic for absorption measurements. Drying was used for flame- and
 107 atomizer-generated particles. A differential mobility analyzer (DMA) and aerosol particle mass
 108 analyzer (APM) were used for particle mobility- and mass-classification, respectively.
 109 Absorption spectra were measured using a broadband photoacoustic spectrometer (PA). Particle
 110 number concentration was measured using a condensation particle counter (CPC).

111 112 2.1 Aerosol generation

113 Carbon black (0.25 mg mL⁻¹, Cab-O-Jet[®] 200, Cabot Corp., Lot # 3404296) [24], graphene
 114 nanoplatelets (4 mg mL⁻¹, Graphene Supermarket #A-12) and fullerene soot (4 mg mL⁻¹, Alfa-

115 Aesar #40971) particles were generated from aqueous solution in a constant-output liquid-jet
116 cross-flow atomizer (TSI 3076) supplied with dry air (dew point < -73 °C) at 30 psig. Of the
117 2.2 L min^{-1} of generated flow, 0.5 L min^{-1} was sampled for measurements while the remainder
118 was exhausted in a laboratory snorkel. For generation of thermally reduced graphene oxide
119 (rGO) [25], graphene oxide (GO, 4 mg mL^{-1} , ACS Material, LLC) was atomized from aqueous
120 solution. After drying, the aerosol stream was passed through a tube furnace (Lindberg-Blue
121 Mini-Mite) at 320 °C to thermally reduce the GO. Any additional water produced during
122 reduction was removed via passage through a secondary drying stage. For generation of
123 graphene nanoplatelets and fullerene soot particles, the supply bottle was immersed in an
124 ultrasonicator during atomization to mechanically suspend material in solution.

125 Fullerene (C_{60}) particles were generated through vaporization and condensation of powdered
126 C_{60} (SES Research #600-9969) in a tube furnace maintained at 650 °C in a flow of Ar at
127 1.5 L min^{-1} [26]. No drying elements were used. Of the supplied flow, 0.5 L min^{-1} was sampled
128 for measurements with the remainder exhausted in a laboratory snorkel.

129 Particles from ethylene fuel were generated from a Santoro diffusion flame [27]. Particles
130 were aspirated into 5 L min^{-1} of dry, HEPA-filtered air via a 1 mm diameter inlet on a sampling
131 tube located 5 cm above burner centerline. An ejector pump located downstream mixed the
132 particle stream with an additional 10 L min^{-1} of dry HEPA-filtered air. Of this flow, 0.5 L min^{-1}
133 was sampled for measurements with the remainder exhausted in a fume hood.

134 Particles from kerosene and diesel fuel were generated from a simple wick lamp made in-
135 house and modeled after typical sources used in developing countries [28, 29]. The simple wick
136 lamp was fueled with USA grade 1-K Kerosene (Klean Strip) or ultra-low sulfur diesel (NIST
137 Emergency Services Facility fueling station, Gaithersburg, MD) using a 3.175 mm diameter

138 braided cotton wick (Pepperell Braiding Company #1115-S) maintained at 1.0 to 1.5 mm above
139 the lip of the lamp. The lamp was operated inside a 56 cm long, 8.25 cm I.D. glass shroud with >
140 50 L min⁻¹ of sheath flow. Under these conditions, the flame height was \approx 1 cm. Particles were
141 sampled through an inlet 2.54 cm in diameter directed downward towards the flame, located \approx
142 7.5 cm above the wick terminus and drawing 0.5 L min⁻¹ of flow. Excess flow was exhausted in
143 a laboratory snorkel.

144 Particles from paraffin wax were generated from candles poured in-house using wax obtained
145 from King of Heaven candles (Rok Ind. Ltd., Nairobi, Kenya) and a 3.175 mm diameter braided
146 cotton wick (Pepperell Braiding Company #1115-S). Wicks were maintained at \approx 1.25 cm during
147 combustion and particles were sampled similarly to the liquid-fuel simple wick lamps.

148 *2.2 Aerosol conditioning and classification*

149 Water was removed prior to particle size- and mass-classification by passing the aerosol
150 stream through a large-diameter Nafion drying tube (Perma Pure, LLC #MD-700-48F-1) with a
151 20:1 parallel flow of dry air (< 5 % relative humidity) and a pair of silica gel diffusion dryers
152 (TSI #3062) prior to size (electrical mobility) selection by a DMA (TSI Long DMA #3081). The
153 relative humidity inside the DMA was monitored to ensure it was stable (< 10 % relative
154 humidity) for the duration of an experiment to avoid interferences from both gas and liquid
155 water [16, 30, 31]. Sheath:aerosol flow in the DMA was maintained at 10:1 by the recirculating
156 pumps in the electrostatic classifier (TSI #3082). After size selection, particles were passed
157 through an APM (Kanomax #3602), a PA and a CPC (TSI #3775) in series. To ensure only
158 particles bearing $q = +1$ were measured by the PA [32], we followed recommendations put forth
159 in Radney and Zangmeister (2016) [33] for tandem DMA/APM measurements.

160 For C₆₀ (generated in Ar), the DMA was operated in a single-pass mode. Dry, HEPA-filtered
161 air was supplied from a compressed air line and removed via vacuum pump with the
162 sheath:aerosol volumetric flow maintained at 10:1 using a pair of mass flow controllers (MKS
163 #1179C). The resulting sample airstream exiting the DMA contained $\approx 10\%$ Ar.

164 2.3 Photoacoustic spectroscopy

165 MAC spectra spanning $\lambda = 500$ nm to 840 nm were measured using a PA equipped with a
166 supercontinuum laser and tunable wavelength and bandpass filter, as in Radney and Zangmeister
167 (2015) [16] and the Supporting Information of Radney, et al. (2017) [34]. Absorption
168 coefficients (α_{abs}), mass (m_p) and particle number densities (N) were calculated from 1 Hz data
169 and averaged to 30 s; wavelength regions were alternated at 30 s intervals. In total, 3 spectra
170 were collected and averaged to a single replicate. For each replicate, MAC at each wavelength
171 was then calculated through the second form of Eq. 1 ($MAC = \alpha_{abs}/m_p N$). MAC values from a
172 minimum of 3 replicates were averaged for all reported spectra; reported measurement
173 uncertainties represent 2 times the standard deviation of all replicates at a given wavelength.
174 From these measurements, material effective density (ρ_{eff}) was also determined ($\rho_{eff} = 6m_p/\pi D_m^3$)
175 where D_m is the particle mobility diameter. Prior to measurement of C₆₀ aerosol, the frequency
176 response of the acoustic resonator was measured to determine the resonant frequency, resonance
177 half width and quality factor to account for changes in the speed of sound due to the higher Ar
178 concentration; see Gillis, et al. (2010) [35].

179 2.4 Particle imaging

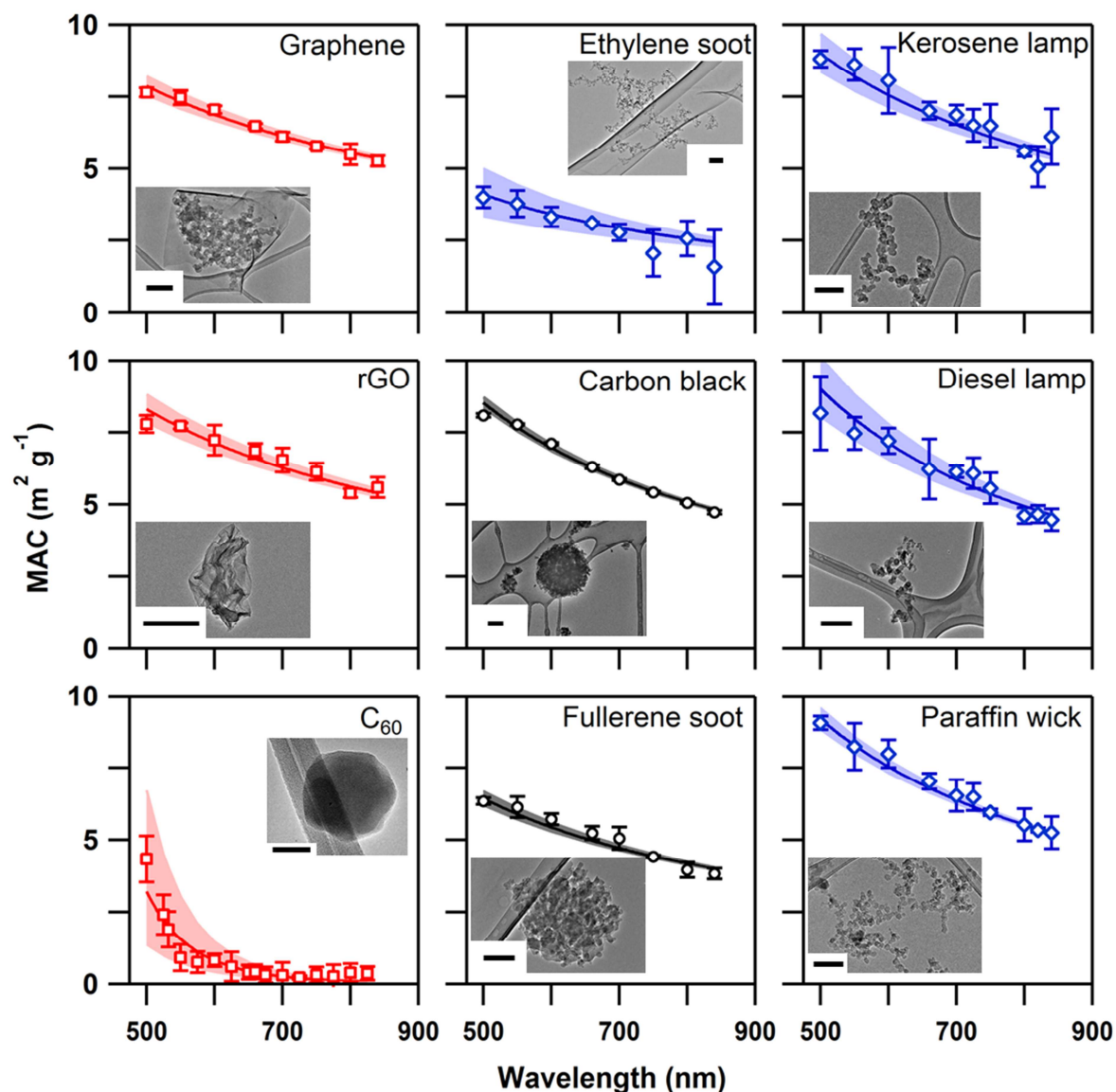
180 For TEM imaging, particles were collected on lacey carbon grids using an electrostatic
181 precipitator at 0.5 L min⁻¹ flow and 8 kV collection voltage. TEM images were collected at an
182 accelerating voltage of 20 keV.

ACCEPTED MANUSCRIPT

184 3. Results and discussion

185 This investigation focuses on the measurement of highly-absorbing carbonaceous aerosol
186 absorption spectra with known electrical mobility diameter (D_m), mass (m_p), and monomer
187 diameters (D_{mon} , where appropriate). Water was removed prior to analysis and no coatings were
188 added to the particles after they were formed [17]. The materials were generated from a variety
189 of sources to quantitatively measure the variability in *MAC* spectra, as shown in Figure 3. Nine
190 forms of highly-absorbing carbonaceous aerosol were measured: two carbon allotropes (C_{60} and
191 crumpled graphene sheets) and seven types of amorphous carbon consisting of spark-discharge
192 fullerene soot [36], thermally reduced graphene oxide (rGO), carbon black, and particles
193 generated from gas (ethylene), liquid (kerosene and diesel) and solid (paraffin) fuel sources.
194 Absorption spectra for each material were measured at the maximum α_{abs} (maximum $\alpha_{abs} =$
195 NC_{abs} for each sample) where the desired $q = +1$ particles could be isolated from the polydisperse
196 distribution [33]. Note that the spectral response of some of the measured materials may be
197 dependent on particle size (electrical mobility), monomer size and/or sheet lateral dimensions,
198 see discussion below. Particles from each sample were collected on lacey carbon grids for TEM
199 imaging; see Figure 3 insets. Additional TEM images are included in the Supplementary Data.
200 Particles from ethylene, kerosene, diesel and paraffin fueled flames possessed lacey aggregate
201 morphologies with low effective densities ($\rho_{eff} < 0.2 \text{ g cm}^{-3}$). The size and distribution of D_{mon}
202 was determined from TEM images of each material and was fuel type dependent, see Table 1.
203 Water-soluble carbon black particles were generated from combustion of carbonaceous fuels
204 followed by rapid surface oxidization. The resulting particles consisted of well-defined
205 aggregated monomers arranged into a nearly-spherical morphology with $\rho_{eff} = 0.77 \text{ g cm}^{-3}$,
206 similar in structure to compacted or aged flame-generated particles observed in the atmosphere

207 and laboratory [3-5, 37, 38]. Fullerene soot was formed from the spark discharge of elemental
208 carbon in the absence of O₂ forming particles with comparable morphology and effective density
209 to carbon black [39], but with oblong, necked, and poorly-defined monomers preventing the
210 determination of D_{mon} . Similar to previous studies [6-9], rGO was composed of multilayered
211 graphene-like sheets with a crumpled nanopaper morphology. Graphene aerosol possessed a
212 similar morphology to rGO with the addition of some soot-like aggregated monomers produced
213 during the formation process. C₆₀ aerosol was arranged into close packed spheres (packing
214 density = 0.73) [26].



215
216

217 **Figure 3.** Plot of mass absorption coefficients (MAC) for the measured particles; corresponding
 218 mobility diameters (D_m) and mass (m_p) are shown in in Table 1. All plots have the same abscissa
 219 and ordinate axis ranges. Uncertainties are 2 times the standard deviation of a minimum of 3
 220 replicate measurements. Red squares are carbon allotropes, black circles are commercially
 221 available materials, and blue diamonds are from laboratory generated particles from flames.
 222 Solid line is AAE determined from Eq. 2. Shaded areas represent fit uncertainties in $MAC_{\lambda,0}$ and
 223 AAE , see Table 1. Insets in each plot show the corresponding TEM images. Scale bars are 200
 224 nm.

225 **Table 1:** Measured mobility diameter (D_m), mass (m_p), effective density (ρ_{eff}), mean monomer
 226 diameter (D_{mon}), measured MAC ($\lambda = 550$ nm), fit $MAC_{\lambda,0}$ ($\lambda_0 = 840$ nm, see Eq. 2) and AAE for
 227 all particle types. Uncertainties shown in parenthesis are 2σ . Green (red) text indicates species
 228 does (does not) meet definition for BC from Ref [18].

Species	D_m (nm)	m_p ($\times 10^{-15}$ g)	ρ_{eff} (g cm^{-3})	D_{mon} (nm)	$MAC_{Measured}$ ($\lambda = 550$ nm)	$MAC_{\lambda,0}$ ($\lambda = 840$ nm)	AAE
Ethylene soot	250	1.47	0.18	17 (3)	3.8 (0.5)	2.4 (0.2)	1.0 (0.3)
Kerosene lamp	700	21.0	0.12	42 (12)	8.6 (0.6)	5.5 (0.2)	1.0 (0.1)
Diesel lamp	700	21.0	0.12	26 (8)	7.5 (0.6)	4.6 (0.2)	1.3 (0.2)
Paraffin wick	700	23.6	0.13	28 (11)	8.2 (0.8)	5.2 (0.1)	1.1 (0.1)
Carbon black ^a	250	6.15	0.77	27 (7)	7.78 (0.06)	4.80 (0.04)	1.11 (0.03)
Graphene	450	23.5	0.51	--	7.5 (0.1)	5.35 (0.08)	0.74 (0.05)
Reduced GO	250	6.40	0.82	--	7.7 (0.1)	5.4 (0.1)	0.83 (0.07)
Fullerene soot	350	16.6	0.74	--	6.1 (0.4)	3.99 (0.06)	0.92 (0.05)
C_{60}	150	2.20	1.2	--	0.9 (0.5)	0.07 (0.02)	7.5 (0.9)

229

230 ^a H_2O soluble material. Does not meet operational definition of BC given in Ref [18].

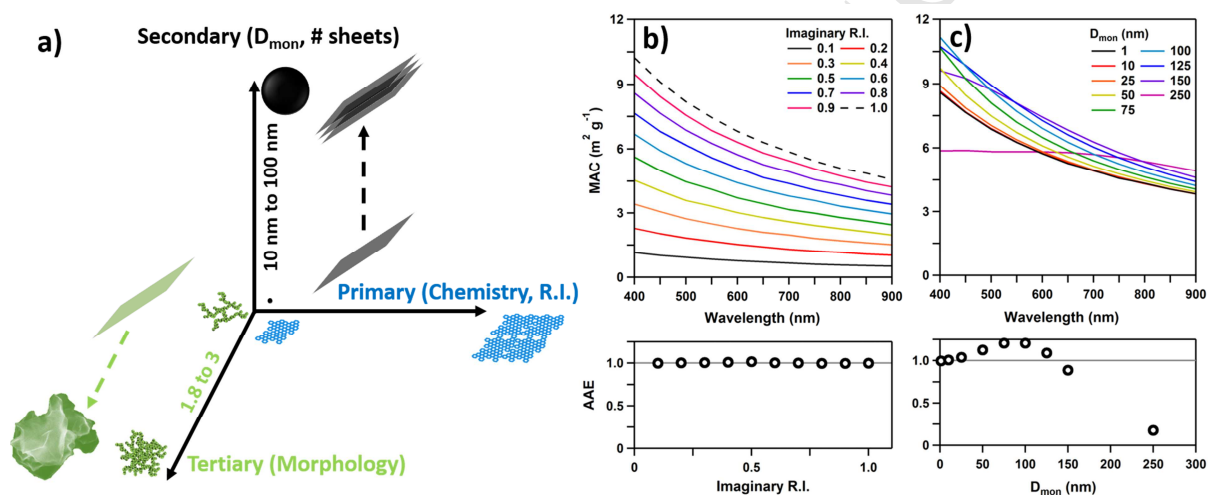
231

232

233 Mass absorption spectra were measured between $\lambda = 500$ nm and 840 nm (see Figure 3) using
 234 a photoacoustic spectrometer and a broadband supercontinuum laser source [16]. Particles
 235 atomized from aqueous solution had a factor of ≈ 5 lower uncertainty than particles generated
 236 from flames. All spectra possessed a minimum of 8 data points allowing for AAE to be fit using
 237 Eq. 2. The MAC at $\lambda = 550$ nm ranged between $0.9 \text{ m}^2 \text{ g}^{-1}$ and $8.6 \text{ m}^2 \text{ g}^{-1}$ (see Table 1). The
 238 measured MAC of carbon black, rGO and graphene were within 2σ of particles generated from
 239 lamp and wick sources at $\lambda = 550$ nm, however their measured AAE 's were not. C_{60} had a MAC
 240 and AAE of $0.9 \pm 0.5 \text{ m}^2 \text{ g}^{-1}$ and 7.5 ± 0.9 , respectively, that exhibited a statistically significant
 241 difference from all other materials.

242 The MAC of flame-generated particles (ethylene, kerosene, diesel, and paraffin) ranged
 243 between $3.8 \text{ m}^2 \text{ g}^{-1}$ and $8.6 \text{ m}^2 \text{ g}^{-1}$; the MAC of particles generated from ethylene were statistically
 244 different than the measured MAC of other flame-generated particles. The AAE of particles
 245 generated from diesel fueled simple wick lamps were also statistically different from the other
 flame-generated particles ($p < 0.05$).

246 It has been noted that the *MAC* of particles produced from high-temperature flames, such as
 247 ethylene, are highly variable due to the quenching of particle oxidation by a rapidly flowing, cool
 248 gas at the flame terminus [3, 16, 40]. Small changes in particle formation conditions can greatly
 249 impact particle concentrations and spectral properties [3]. The *MAC* for ethylene presented in
 250 this study are comparable to previous reports in this laboratory using fuel flow conditions where
 251 particle concentration and α_{abs} were maximized and intra- and inter-day variability and
 252 uncertainty in *MAC* were minimized [3, 37].



253
 254
 255 **Figure 4.** a) Mass absorption coefficients (*MAC*) of carbonaceous particles are a function of
 256 primary (refractive index), secondary (atomistic arrangement), and tertiary structures (particle
 257 morphology). b) *MAC* and absorption Ångström exponent (*AAE*) as a function of imaginary
 258 component of the refractive index for particles with a real component of the refractive index =
 259 1.77, 1 nm monomer diameter (D_{mon}) and 1.65 g cm^{-1} mass density. c) *MAC* and *AAE* as a
 260 function of D_{mon} at constant refractive index ($m = 1.77 + 0.8i$).
 261

262 The parameters that influence the spectroscopy of graphene-like materials in spherical
 263 structures with a high imaginary component of the refractive index (k) has been previously
 264 described in detail by Moosmüller, et al. [10, 11]. It is important to note that the measured
 265 absorption per unit mass of highly-absorbing carbonaceous aerosol is a function the primary,
 266 secondary and tertiary structures of the material [41-44]; see Figure 4a. The intrinsic absorption
 267 strength of a material is a function of its chemical composition (i.e. refractive index); for

268 graphitic and graphenic materials, this refers to the extent of sp^2 -bonding, surface imperfections
269 and single sheet lateral dimension. Absorption by the primary structures can be enhanced or
270 dampened depending upon their atomistic arrangement into secondary structure(s) as spheres,
271 multilayered sheets, etc. The collection of secondary structures into a final tertiary morphology
272 can further impact absorption strength. Figure 4b shows Mie theory calculations that simulate the
273 effect of material primary structure (chemistry) on absorption strength per unit mass (MAC) by
274 changing the imaginary component of the refractive index (k) with a constant real component (n
275 $= 1.77$); monomer diameter ($D_{mon} = 1$ nm) and mass density ($\rho = 1.65$ g cm^{-3}); this D_{mon} and ρ
276 approximates a single C_{60} molecule. In this case, MAC increases monotonically with k and the
277 spectral shape is invariant, $AAE = 1.0$, for all values of k .

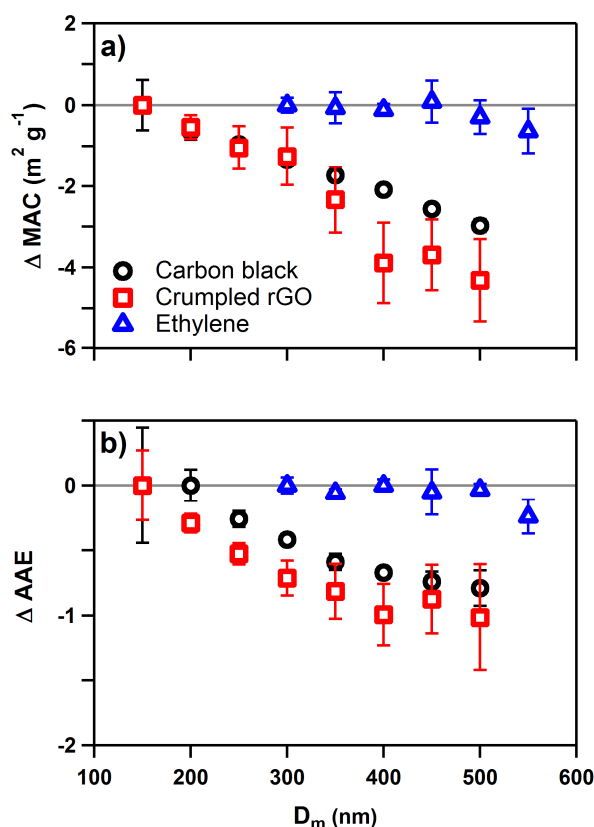
278 The effect of secondary structure on MAC was also simulated for a spherical particle by
279 changing monomer diameter (D_{mon}) at a constant refractive index ($m = 1.77 + 0.8i$) and mass
280 density ($\rho = 1.65$ g cm^{-3}); see Figure 4c. At $\lambda = 400$ nm the MAC increases by 1 percent between
281 a D_{mon} of 1 nm and 10 nm and 13 percent between 10 nm and 50 nm. For this refractive index,
282 monomers ≥ 10 nm in diameter are outside of the volume absorption regime (constant MAC).
283 The results also show AAE increasing from 1.0 to 1.2 for D_{mon} between 1 nm and 100 nm. For
284 $D_{mon} \geq 100$ nm, the spectral dependence may not be adequately captured by an AAE (Eq. 2).

285 The effect of tertiary structure (i.e. morphology) on MAC for a collection of monomers is
286 also significant. However, calculating MAC with elaborate particle geometries is a computational
287 challenge best addressed using complex optical routines such as the discrete dipoles
288 approximation and the superposition T-matrix method as described in studies by Mishchenko
289 and Mackowski, among others [45-49].

290 These Mie theory calculations assume the simplest case using monodisperse spherical
291 monomers, but help to capture the complexity and challenge of quantitative measurement,
292 reporting, and comparison of highly-absorbing carbonaceous aerosol spectral data. In this
293 investigation, the D_{mon} of flame-generated particles ranged between 17 nm (ethylene soot) and 42
294 nm (kerosene lamp). Mie theory calculations over this range show that the MAC and AAE
295 increase nearly linearly with D_{mon} at constant refractive index (see Supplemental Data Figure
296 S3), with the MAC and AAE of 42 nm diameter monomers nearly 6 percent and 12 percent higher
297 than 17 nm monomers, respectively. Thus, the difference in MAC and AAE between particles
298 generated from ethylene fueled flames and wick lamps, with the only difference being the fuel
299 used, cannot be explained solely by D_{mon} . As all flame-generated particles had comparable
300 morphology, the measured differences in MAC and AAE are likely due to differences in the
301 refractive indices of each material under the measured formative conditions.

302 The definition of BC has 4 measurable properties [18]: 1) composed of aggregates of small
303 carbon spherules, 2) $MAC \geq 5 \text{ m}^2 \text{ g}^{-1}$ at $\lambda = 550 \text{ nm}$, 3) refractory with a vaporization temperature
304 near 4000 K, 4) insoluble in water and common organic solvents. Properties 1 and 2 were
305 directly measured in this investigation. Despite some materials having formative conditions
306 consistent with BC, only three of the nine samples met both the morphological and spectroscopic
307 definitions of BC (particles generated from kerosene and diesel lamps, and the paraffin wax
308 candle), see green text in Table 1. The particles produced in this investigation from an ethylene
309 fueled flame did not meet the spectroscopic definition for BC, whereas graphene and rGO did
310 not meet the morphological definition. Carbon black met the morphological and spectroscopic
311 definitions but its water solubility negates its inclusion.

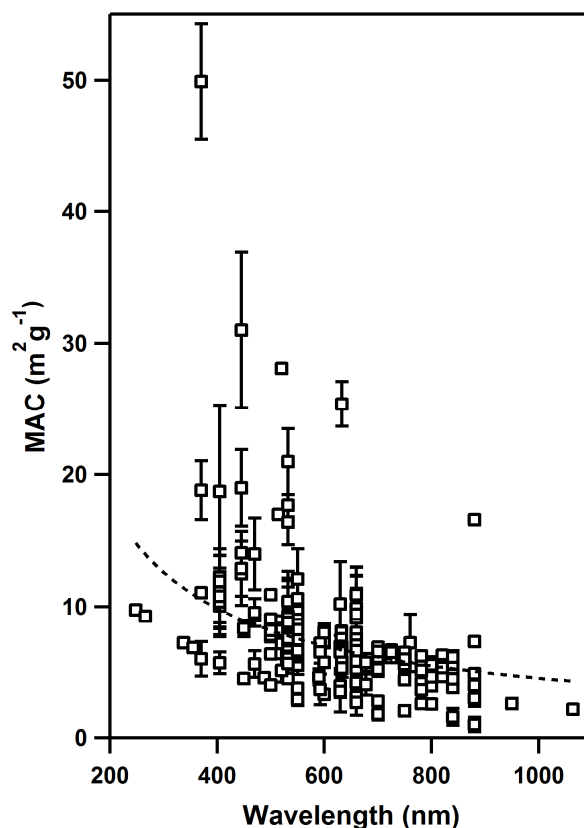
312
313



314
 315 **Figure 5.** a) Change (Δ) in the mass absorption coefficient (MAC) at $\lambda = 532$ nm and b) change
 316 (Δ) in absorption Ångström exponent (AAE) between $\lambda = 532$ nm and 780 nm as function of
 317 particle mobility diameter (D_m) for compact carbon black (red squares), crumpled rGO (black
 318 circles), and fresh, lacey particles from ethylene flame (blue circles). Error bars are 1 standard
 319 deviation of a minimum of 3 replicate measurements.

320
 321 As shown in Figure 4a, in addition to being dependent on material refractive index and D_{mon} ,
 322 MAC is also a function of morphology and/or D_m . It can be envisioned that particles with a lacey
 323 morphology – e.g. freshly-emitted flame-generated particles – with small D_{mon} enables light to
 324 access the entire particle resulting in absorption that scales linearly with particle mass (volume)
 325 for all D_m . In contrast, particles with a compacted morphology may only be in the volume
 326 absorption regime (constant MAC and AAE) at very small mobility diameters (D_m) and transition
 327 to the Mie or geometric absorption regimes with increasing D_m , resulting in both parameters
 328 being a function of D_m . Figure 5 tests this hypothesis by measuring the change (Δ) in MAC and
 329 AAE as a function of D_m between $\lambda = 532$ nm and 780 nm for mass- and mobility-selected

330 particles (21 samples) of multilayered crumpled sheets (rGO), compacted flame-generated
331 particles (carbon black) and freshly formed, lacy particles generated from an ethylene flame
332 with $D_{mon} \approx 20$ nm. Particles generated from the ethylene flame were measured between 300 nm
333 $\leq D_m \leq 550$ nm where it was assured only singly-charged particles were isolated from the
334 distribution [3, 33]. The *MAC* of the crumpled sheets and compacted spherical particles
335 decreases nearly monotonically with D_m , consistent with geometric absorption even for the
336 smallest particles measured ($D_m = 150$ nm). A similar dependence was measured for the change
337 in *AAE* with D_m for crumpled and compacted particles, see Figure 4b. For particles generated
338 from an ethylene flame, the *MAC* and *AAE* are constant within measurement uncertainty for
339 particles up to $D_m = 550$ nm and typical of particles in the volumetric absorption regime. These
340 data confirm that particle morphology impacts the spectral properties of highly-absorbing
341 carbonaceous particles. For flame-generated particles where D_{mon} is small and the morphology is
342 consistent with an open, lacy structure (fractal dimension, $D_f \approx 1.8$ [50]) it is reasonable to
343 assume that the particle absorption scales directly with particle mass and *MAC* and *AAE* are
344 invariant. For particles that fall outside of this narrow parameter space this assumption may not
345 be valid.



346
 347
 348 **Figure 6.** All published *MAC* data of BC, soot and allotropes of carbon between 1971 to current
 349 as a function of wavelength. Error bars are 1σ . Dashed line is fit to Eq. 2 – Data from refs. [3, 12,
 350 36, 38, 51-77].
 351

352 Many studies have focused on the measurement and reporting of *MAC* for highly-absorbing
 353 carbonaceous (BC-like) particles in the atmosphere since the first assessment of BC *MAC* [1].
 354 Figure 6 shows the absorption spectra collected in this investigation, with the exception of C_{60} ,
 355 and all the peer-reviewed *MAC* data (1971 to 2018, 199 measured values) for materials reported
 356 as BC or soot, including 26 measurements of graphite and graphene allotropes of carbon [3, 12,
 357 36, 38, 51-77]. The reported data include both laboratory measurements of characterized systems
 358 from known sources such as coal combustion, kerosene wick lamps, diesel engines, diffusion
 359 flames, and spark discharge soot with known carbon-to-oxygen ratios and data from field-based
 360 observations from sites such as traffic tunnels and urban areas. The data are shown at the

361 wavelength reported in each study with 1σ uncertainty (if reported). The published data include
 362 129 *MAC* values measured using photoacoustic spectroscopy (PAS), 36 reports from filter-based
 363 methods, and 29 reports which used extinction minus scattering. The range of data extends from
 364 $248 \text{ nm} \leq \lambda \leq 1064 \text{ nm}$, enabling the use of Eq. 2 to determine *AAE* and *MAC*.

365 The *MAC* of the previously published data is highly variable. For example, at $\lambda = 532 \text{ nm}$ (24
 366 samples) the *MAC* of all published data ranges between $5.61 \pm 0.46 \text{ m}^2 \text{ g}^{-1}$ and $21.0 \pm 2.5 \text{ m}^2 \text{ g}^{-1}$,
 367 (average = $8.31 \pm 0.89 \text{ m}^2 \text{ g}^{-1}$) larger than the variability in *MAC* for the carbonaceous materials
 368 measured in this study. The published data was also examined by the source of the material.
 369 Aerosol generated from diesel engines represents the largest single source of reported *MAC* data
 370 (19 reported *MAC* values). The reported range in *MAC* from diesel engine generated aerosol for
 371 $514 \text{ nm} \leq \lambda \leq 532 \text{ nm}$ (7 samples) is $7.4 \pm 0.5 \text{ m}^2 \text{ g}^{-1}$ to $17 \text{ m}^2 \text{ g}^{-1}$ (no reported uncertainty) with
 372 an average of $9.5 \pm 3.3 \text{ m}^2 \text{ g}^{-1}$.

373 The *AAE* of the all data shown in Figure 6 was calculated using Eq. 2 as 1.01 ± 0.15 (1σ),
 374 within uncertainty of 1.0 suggested in Bond and Bergstrom (2006) and in support of the λ^{-1}
 375 dependence [1, 3, 10, 11, 18]. The *MAC* of the population using all the published data at $\lambda = 550$
 376 nm is $8.28 \pm 0.34 \text{ m}^2 \text{ g}^{-1}$, 10 percent higher than the previous assessment of BC *MAC*, with
 377 uncertainty reduced by a factor of 4, see Table 2.

378 **Table 2.** Fit parameters calculated from Eq. 2 of published carbonaceous aerosol *MAC* between
 379 1971 and 2018. Fit parameters also reported for published PAS and filter-based measurements
 380 and after removal of outlier data $> 5\sigma$ from mean. Uncertainties are 1σ and shown in parenthesis.

	k_0 ($\lambda = 550 \text{ nm}$, $\text{m}^2 \text{ g}^{-1}$)	<i>AAE</i>
All published measurements	8.28 (0.34)	1.01 (0.15)
All published PAS	8.03 (0.31)	0.84 (0.13)
All published Filter-based	9.67 (1.50)	1.83 (0.56)
All measurements – 5σ outliers removed	7.52 (0.18)	0.85 (0.09)
PAS – 5σ outliers removed	7.39 (0.19)	0.76 (0.19)
Filter-based – 5σ outliers removed	7.40 (0.53)	1.31 (0.28)

381

382 Some of the published *MAC* data was more than 5σ from the mean, greatly increasing the
383 uncertainty in both *AAE* and *MAC*, and are likely not physical (e.g. $MAC = 50 \text{ m}^2 \text{ g}^{-1}$ at $\lambda = 370$
384 nm) based on *MAC* calculated from refractive indices and D_{mon} using Mie theory. The published
385 data shows a dependence on the method utilized for analysis, see Table 2. For example, using
386 only PAS data yields $MAC = 8.03 \pm 0.31 \text{ m}^2 \text{ g}^{-1}$ and $AAE = 0.84 \pm 0.13$, whereas using data from
387 filter-based studies results in $MAC = 9.67 \pm 1.50 \text{ m}^2 \text{ g}^{-1}$ and $AAE = 1.83 \pm 0.56$. Curation of all
388 the data via elimination of data outside of the average $MAC + 5\sigma$ (9 points removed) results in a
389 50 percent reduction in the reported uncertainty for the *MAC*, with $MAC = 7.52 \pm 0.18 \text{ m}^2 \text{ g}^{-1}$ and
390 $AAE = 0.85 \pm 0.09$, within 1σ of *MAC* but with a lower *AAE* than reported in the BC assessments
391 [1, 18].

392 4. Conclusions

393 The presented data highlight *MAC* variability of highly-absorbing carbonaceous aerosol. BC
394 has been previously defined as a material with a well-defined refractive index and *MAC* that can
395 be assigned defined values (e.g. BC refractive index = $1.95 + 0.79i$, $MAC = 7.5 \pm 1.2 \text{ m}^2 \text{ g}^{-1}$) [1],
396 similar to other well-defined nanomaterials such as SiO_2 or polystyrene spheres that have been
397 used for standards. If a single *MAC* value exists for BC and other similar materials, it would be
398 expected that its reported range would be narrow; see data at $\lambda = 532 \text{ nm}$ and 660 nm in Figure 6
399 where adequate data exists for comparison between studies. The range in published *MAC*
400 observations suggests that either: 1) the reported data is dominated by measurement errors and
401 biases and that the *MAC* of BC and other similar materials is well-defined and invariant across
402 formative conditions or 2) the reported data captures the spectral variability and that highly-
403 absorbing carbonaceous aerosol exists within a range of chemical and physical properties that
404 impact particle absorption. Based on the measurements presented in this study for particles with

405 known D_m , D_{mon} , m_p , and morphology it is likely the observed spectral variability in highly-
406 absorbing carbonaceous aerosol is due to the impact of material refractive index, D_{mon} , and, in
407 some cases, particle morphology that result from the diversity of formative conditions for this
408 family of materials.

409 **Acknowledgements**

410 The authors thank Yong Yang at the University of Maryland for assistance in acquisition of
411 TEM images of some of samples.

412 **Appendix A. Supplementary Data**

413 Supplementary Data includes Mie theory calculations of MAC and as a function of D_{mon} , and
414 TEM images of particles.

415 416 **References**

- 417
418 [1] T.C. Bond, R.W. Bergstrom, Light absorption by carbonaceous particles: An
419 investigative review, *Aerosol Sci. Technol.* 40 (1) (2006) 27-67.
420 [2] P.R. Buseck, K. Adachi, A. Gelencsér, É. Tompa, M. Pósfai, Ns-soot: A material-based
421 term for strongly light-absorbing carbonaceous particles, *Aerosol Sci. Technol.* 48 (7) (2014)
422 777-788.
423 [3] J.G. Radney, R. You, X. Ma, J.M. Conny, M.R. Zachariah, J.T. Hodges, et al.,
424 Dependence of soot optical properties on particle morphology: Measurements and model
425 comparisons, *Environ. Sci. Technol.* 48 (6) (2014) 3169-3176.
426 [4] X. Ma, C.D. Zangmeister, J. Gigault, G.W. Mulholland, M.R. Zachariah, Soot aggregate
427 restructuring during water processing, *J. Aerosol Sci.* 66 (2013) 209-219.
428 [5] J. Peng, M. Hu, S. Guo, Z. Du, J. Zheng, D. Shang, et al., Markedly enhanced absorption
429 and direct radiative forcing of black carbon under polluted urban environments, *Proc. Natl.*
430 *Acad. Sci. U. S. A.* 113 (16) (2016) 4266-4271.
431 [6] X. Ma, M.R. Zachariah, C.D. Zangmeister, Crumpled nanopaper from graphene oxide,
432 *Nano Lett.* 12 (1) (2011) 486-489.
433 [7] X. Ma, M.R. Zachariah, C.D. Zangmeister, Reduction of suspended graphene oxide
434 single sheet nanopaper: The effect of crumpling, *J. Phys. Chem. C* 117 (6) (2013) 3185-3191.
435 [8] W.-N. Wang, Y. Jiang, P. Biswas, Evaporation-induced crumpling of graphene oxide
436 nanosheets in aerosolized droplets: Confinement force relationship, *J. Phys. Chem. Lett.* 3 (21)
437 (2012) 3228-3233.
438 [9] H. Yang, Y. Wang, Y. Song, L. Qiu, S. Zhang, D. Li, et al., Assembling of graphene
439 oxide in an isolated dissolving droplet, *Soft Matter* 8 (44) (2012) 11249-11254.

- 440 [10] H. Moosmüller, W.P. Arnott, Particle optics in the rayleigh regime, *J. Air Waste*
441 *Manage. Assoc.* 59 (9) (2009) 1028-31.
- 442 [11] H. Moosmüller, R.K. Chakrabarty, W.P. Arnott, Aerosol light absorption and its
443 measurement: A review, *J. Quant. Spectrosc. Radiat. Transfer* 110 (11) (2009) 844-878.
- 444 [12] H. Moosmüller, W.P. Arnott, C.F. Rogers, J.C. Chow, C.A. Frazier, L.E. Sherman, et
445 al., Photoacoustic and filter measurements related to aerosol light absorption during the northern
446 front range air quality study (colorado 1996/1997), *J. Geophys. Res.: Atmos.* 103 (D21) (1998)
447 28149-28157.
- 448 [13] B. Srinivas, N. Rastogi, M.M. Sarin, A. Singh, D. Singh, Mass absorption efficiency of
449 light absorbing organic aerosols from source region of paddy-residue burning emissions in the
450 indo-gangetic plain, *Atmos. Environ.* 125, Part B (2016) 360-370.
- 451 [14] R.K. Chakrabarty, M. Gyawali, R.L.N. Yatavelli, A. Pandey, A.C. Watts, J. Knue, et al.,
452 Brown carbon aerosols from burning of boreal peatlands: Microphysical properties, emission
453 factors, and implications for direct radiative forcing, *Atmos. Chem. Phys.* 16 (5) (2016) 3033-
454 3040.
- 455 [15] L. Caponi, P. Formenti, D. Massabó, C. Di Biagio, M. Cazaunau, E. Pangui, et al.,
456 Spectral- and size-resolved mass absorption efficiency of mineral dust aerosols in the shortwave
457 spectrum: A simulation chamber study, *Atmos. Chem. Phys.* 17 (11) (2017) 7175-7191.
- 458 [16] J.G. Radney, C.D. Zangmeister, Measurement of gas and aerosol phase absorption
459 spectra across the visible and near-ir using supercontinuum photoacoustic spectroscopy, *Anal.*
460 *Chem.* 87 (14) (2015) 7356-7363.
- 461 [17] R. You, J.G. Radney, M.R. Zachariah, C.D. Zangmeister, Measured wavelength-
462 dependent absorption enhancement of internally mixed black carbon with absorbing and
463 nonabsorbing materials, *Environ. Sci. Technol.* 50 (15) (2016) 7982-7990.
- 464 [18] T.C. Bond, S.J. Doherty, D.W. Fahey, P.M. Forster, T. Berntsen, B.J. DeAngelo, et al.,
465 Bounding the role of black carbon in the climate system: A scientific assessment, *J. Geophys.*
466 *Res.: Atmos.* 118 (2013) 5380 - 5552.
- 467 [19] V. Ramanathan, G. Carmichael, Global and regional climate changes due to black
468 carbon, *Nat. Geosci.* 1 (4) (2008) 221-227.
- 469 [20] T. Ajtai, N. Utry, M. Pintér, B. Major, Z. Bozóki, G. Szabó, A method for segregating
470 the optical absorption properties and the mass concentration of winter time urban aerosol,
471 *Atmos. Environ.* 122 (2015) 313-320.
- 472 [21] N. Utry, T. Ajtai, Á. Filep, M. Pintér, Z. Török, Z. Bozóki, et al., Correlations between
473 absorption angstrom exponent (aae) of wintertime ambient urban aerosol and its physical and
474 chemical properties, *Atmos. Environ.* 91 (2014) 52-59.
- 475 [22] D. Baumgardner, O. Popovicheva, J. Allan, V. Bernardoni, J. Cao, F. Cavalli, et al.,
476 Soot reference materials for instrument calibration and intercomparisons: A workshop summary
477 with recommendations, *Atmos. Meas. Tech.* 5 (8) (2012) 1869-1887.
- 478 [23] J.G. Slowik, E.S. Cross, J.-H. Han, P. Davidovits, T.B. Onasch, J.T. Jayne, et al., An
479 inter-comparison of instruments measuring black carbon content of soot particles, *Aerosol Sci.*
480 *Technol.* 41 (3) (2007) 295-314.
- 481 [24] NIST technical disclaimer: Certain commercial equipment, instruments, or materials (or
482 suppliers, or software, ...) are identified in this paper to foster understanding. Such identification
483 does not imply recommendation or endorsement by the National Institute of Standards and
484 Technology, nor does it imply that the materials or equipment identified are necessarily the best
485 available for the purpose.

- 486 [25] C.D. Zangmeister, Preparation and evaluation of graphite oxide reduced at 220 °C,
487 Chem. Mater. 22 (19) (2010) 5625-5629.
- 488 [26] A.S. Gurav, T.T. Kodas, L.-M. Wang, E.I. Kauppinen, J. Joutsensaari, Generation of
489 nanometer-size fullerene particles via vapor condensation, Chem. Phys. Lett. 218 (4) (1994) 304-
490 308.
- 491 [27] R.J. Santoro, H.G. Semerjian, R.A. Dobbins, Soot particle measurements in diffusion
492 flames, Combust. Flame 51 (0) (1983) 203-218.
- 493 [28] J. Apple, R. Vicente, A. Yarberry, N. Lohse, E. Mills, A. Jacobson, et al.,
494 Characterization of particulate matter size distributions and indoor concentrations from kerosene
495 and diesel lamps, Indoor Air 20 (5) (2010) 399-411.
- 496 [29] N.L. Lam, Y. Chen, C. Weyant, C. Venkataraman, P. Sadavarte, M.A. Johnson, et al.,
497 Household light makes global heat: High black carbon emissions from kerosene wick lamps,
498 Environ. Sci. Technol. 46 (24) (2012) 13531-13538.
- 499 [30] J.G. Radney, C.D. Zangmeister, Light source effects on aerosol photoacoustic
500 spectroscopy measurements, J. Quant. Spectrosc. Radiat. Transfer 187 (2017) 145-149.
- 501 [31] J.M. Langridge, M.S. Richardson, D.A. Lack, C.A. Brock, D.M. Murphy, Limitations of
502 the photoacoustic technique for aerosol absorption measurement at high relative humidity,
503 Aerosol Sci. Technol. 47 (11) (2013) 1163-1173.
- 504 [32] J.G. Radney, X. Ma, K.A. Gillis, M.R. Zachariah, J.T. Hodges, C.D. Zangmeister,
505 Direct measurements of mass-specific optical cross sections of single component aerosol
506 mixtures, Anal. Chem. 85 (17) (2013) 8319-8325.
- 507 [33] J.G. Radney, C.D. Zangmeister, Practical limitations of aerosol separation by a tandem
508 differential mobility analyzer–aerosol particle mass analyzer, Aerosol Sci. Technol. 50 (2)
509 (2016) 160-172.
- 510 [34] J.G. Radney, R. You, M.R. Zachariah, C.D. Zangmeister, Direct in situ mass specific
511 absorption spectra of biomass burning particles generated from smoldering hard and softwoods,
512 Environ. Sci. Technol. 51 (10) (2017) 5622-5629.
- 513 [35] K.A. Gillis, D.K. Havey, J.T. Hodges, Standard photoacoustic spectrometer: Model and
514 validation using o2 a-band spectra, Rev. Sci. Instrum. 81 (6) (2010) 064902-13.
- 515 [36] M. Schnaiter, H. Horvath, O. Möhler, K.H. Naumann, H. Saathoff, O.W. Schöck, Uv-
516 vis-nir spectral optical properties of soot and soot-containing aerosols, J. Aerosol Sci. 34 (10)
517 (2003) 1421-1444.
- 518 [37] P.A. Bueno, D.K. Havey, G.W. Mulholland, J.T. Hodges, K.A. Gillis, R.R. Dickerson,
519 et al., Photoacoustic measurements of amplification of the absorption cross section for coated
520 soot aerosols, Aerosol Sci. Technol. 45 (10) (2011) 1217-1230.
- 521 [38] R. Zhang, A.F. Khalizov, J. Pagels, D. Zhang, H. Xue, P.H. McMurry, Variability in
522 morphology, hygroscopicity, and optical properties of soot aerosols during atmospheric
523 processing, Proc. Natl. Acad. Sci. U. S. A. 105 (30) (2008) 10291-10296.
- 524 [39] N. Moteki, Y. Kondo, N. Takegawa, S.-i. Nakamura, Directional dependence of thermal
525 emission from nonspherical carbon particles, J. Aerosol Sci. 40 (9) (2009) 790-801.
- 526 [40] R.H. Moore, L.D. Ziemba, D. Dutcher, A.J. Beyersdorf, K. Chan, S. Crumeyrolle, et al.,
527 Mapping the operation of the miniature combustion aerosol standard (mini-cast) soot generator,
528 Aerosol Sci. Technol. 48 (5) (2014) 467-479.
- 529 [41] C. García Fernández, S. Picaud, M. Devel, Calculations of the mass absorption cross
530 sections for carbonaceous nanoparticles modeling soot, J. Quant. Spectrosc. Radiat. Transfer 164
531 (Supplement C) (2015) 69-81.

- 532 [42] R. Langlet, M.R. Vanacharla, S. Picaud, M. Devel, Bottom-up multi-step approach to
533 study the relations between the structure and the optical properties of carbon soot nanoparticles,
534 *J. Quant. Spectrosc. Radiat. Transfer* 110 (14) (2009) 1615-1627.
- 535 [43] F. Moulin, M. Devel, S. Picaud, Optical properties of soot nanoparticles, *J. Quant.*
536 *Spectrosc. Radiat. Transfer* 109 (10) (2008) 1791-1801.
- 537 [44] B.V. Scarnato, S. Vahidinia, D.T. Richard, T.W. Kirchstetter, Effects of internal mixing
538 and aggregate morphology on optical properties of black carbon using a discrete dipole
539 approximation model, *Atmos. Chem. Phys.* 13 (10) (2013) 5089-5101.
- 540 [45] W.R. Heinson, A. Chakrabarti, C.M. Sorensen, Divine proportion shape invariance of
541 diffusion limited cluster-cluster aggregates, *Aerosol Sci. Technol.* 49 (9) (2015) 786-792.
- 542 [46] Y.W. Heinson, J.B. Maughan, W.R. Heinson, A. Chakrabarti, C.M. Sorensen, Light
543 scattering q-space analysis of irregularly shaped particles, *J. Geophys. Res.: Atmos.* 121 (2)
544 (2016) 682-691.
- 545 [47] M.I. Mishchenko, D.W. Mackowski, L.D. Travis, Scattering of light by bispheres with
546 touching and separated components, *Appl. Opt.* 34 (21) (1995) 4589-4599.
- 547 [48] K. Skorupski, The optical properties of tropospheric soot aggregates determined with the
548 dda (discrete dipole approximation) method, *SPIE Optical Metrology*, SPIE, 2015, p. 10.
- 549 [49] C. Sorensen, Y. Heinson, W. Heinson, J. Maughan, A. Chakrabarti, Q-space analysis of
550 the light scattering phase function of particles with any shape, *Atmosphere* 8 (4) (2017) 68.
- 551 [50] C.M. Sorensen, Light scattering by fractal aggregates: A review, *Aerosol Sci. Technol.*
552 35 (2) (2001) 648-687.
- 553 [51] C.W. Bruce, T.F. Stromberg, K.P. Gurton, J.B. Mozer, Trans-spectral absorption and
554 scattering of electromagnetic radiation by diesel soot, *Appl. Opt.* 30 (12) (1991) 1537-1546.
- 555 [52] C.E. Chung, S.W. Kim, M. Lee, S.C. Yoon, S. Lee, Carbonaceous aerosol aae inferred
556 from in-situ aerosol measurements at the gosan abc super site, and the implications for brown
557 carbon aerosol, *Atmos. Chem. Phys.* 12 (14) (2012) 6173-6184.
- 558 [53] I. Colbeck, B. Atkinson, Y. Johar, The morphology and optical properties of soot
559 produced by different fuels, *J. Aerosol Sci.* 28 (5) (1997) 715-723.
- 560 [54] I. Colbeck, E.J. Hardman, R.M. Harrison, Optical and dynamical properties of fractal
561 clusters of carbonaceous smoke, *J. Aerosol Sci.* 20 (7) (1989) 765-774.
- 562 [55] E.S. Cross, T.B. Onasch, A. Ahern, W. Wrobel, J.G. Slowik, J. Olfert, et al., Soot
563 particle studies - instrument inter-comparison - project overview, *Aerosol Sci. Technol.* 44 (8)
564 (2010) 592-611.
- 565 [56] X. Cui, X. Wang, L. Yang, B. Chen, J. Chen, A. Andersson, et al., Radiative absorption
566 enhancement from coatings on black carbon aerosols, *Sci. Total Environ.* 551-552 (Supplement
567 C) (2016) 51-56.
- 568 [57] J. Genberg, H.A.C. Denier van der Gon, D. Simpson, E. Swietlicki, H. Areskoug, D.
569 Beddows, et al., Light-absorbing carbon in europe - measurement and modelling, with a focus on
570 residential wood combustion emissions, *Atmos. Chem. Phys.* 13 (17) (2013) 8719-8738.
- 571 [58] L.A. Gundel, R.L. Dod, H. Rosen, T. Novakov, The relationship between optical
572 attenuation and black carbon concentration for ambient and source particles, *Sci. Total Environ.*
573 36 (Supplement C) (1984) 197-202.
- 574 [59] A.F. Khalizov, H. Xue, L. Wang, J. Zheng, R. Zhang, Enhanced light absorption and
575 scattering by carbon soot aerosol internally mixed with sulfuric acid, *J. Phys. Chem. A* 113 (6)
576 (2009) 1066-1074.

- 577 [60] A. Knox, G.J. Evans, J.R. Brook, X. Yao, C.H. Jeong, K.J. Godri, et al., Mass
578 absorption cross-section of ambient black carbon aerosol in relation to chemical age, *Aerosol*
579 *Sci. Technol.* 43 (6) (2009) 522-532.
- 580 [61] M. Laborde, M. Crippa, T. Tritscher, Z. Jurányi, P.F. Decarlo, B. Temime-Roussel, et
581 al., Black carbon physical properties and mixing state in the european megacity paris, *Atmos.*
582 *Chem. Phys.* 13 (11) (2013) 5831-5856.
- 583 [62] C. Linke, I. Ibrahim, N. Schleicher, R. Hitzenberger, M.O. Andreae, T. Leisner, et al., A
584 novel single-cavity three-wavelength photoacoustic spectrometer for atmospheric aerosol
585 research, *Atmos. Meas. Tech.* 9 (11) (2016) 5331-5346.
- 586 [63] D. Liu, M. Flynn, M. Gysel, A. Targino, I. Crawford, K. Bower, et al., Single particle
587 characterization of black carbon aerosols at a tropospheric alpine site in switzerland, *Atmos.*
588 *Chem. Phys.* 10 (15) (2010) 7389-7407.
- 589 [64] G.W. Mulholland, M.Y. Choi, Measurement of the mass specific extinction coefficient
590 for acetylene and ethene smoke using the large agglomerate optics facility, *Symp. (Int.)*
591 *Combust., [Proc.]* 27 (1) (1998) 1515-1522.
- 592 [65] E.M. Patterson, R.M. Duckworth, C.M. Wyman, E.A. Powell, J.W. Gooch,
593 Measurements of the optical properties of the smoke emissions from plastics, hydrocarbons, and
594 other urban fuels for nuclear winter studies, *Atmos. Environ., Part A* 25 (11) (1991) 2539-2552.
- 595 [66] D.M. Roessler, F.R. Faxvog, Optoacoustic measurement of optical absorption in
596 acetylene smoke, *J. Opt. Soc. Am.* 69 (12) (1979) 1699-1704.
- 597 [67] R. Röhl, W.A. McClenny, R.A. Palmer, Photoacoustic determination of optical
598 properties of aerosol particles collected on filters: Development of a method taking into account
599 substrate reflectivity, *Appl. Opt.* 21 (3) (1982) 375-381.
- 600 [68] G. Saliba, R. Subramanian, R. Saleh, A.T. Ahern, E.M. Lipsky, A. Tasoglou, et al.,
601 Optical properties of black carbon in cookstove emissions coated with secondary organic
602 aerosols: Measurements and modeling, *Aerosol Sci. Technol.* 50 (11) (2016) 1264-1276.
- 603 [69] M. Schnaiter, M. Gimmler, I. Llamas, C. Linke, C. Jäger, H. Mutschke, Strong spectral
604 dependence of light absorption by organic carbon particles formed by propane combustion,
605 *Atmos. Chem. Phys.* 6 (10) (2006) 2981-2990.
- 606 [70] P.J. Sheridan, W.P. Arnott, J.A. Ogren, E. Andrews, D.B. Atkinson, D.S. Covert, et al.,
607 The reno aerosol optics study: An evaluation of aerosol absorption measurement methods,
608 *Aerosol Sci. Technol.* 39 (1) (2005) 1-16.
- 609 [71] P.R. Sinha, Y. Kondo, M. Koike, J.A. Ogren, A. Jefferson, T.E. Barrett, et al.,
610 Evaluation of ground-based black carbon measurements by filter-based photometers at two arctic
611 sites, *J. Geophys. Res.: Atmos.* 122 (6) (2017) 3544-3572.
- 612 [72] T. Smausz, B. Kondász, T. Gera, T. Ajtai, N. Utry, M. Pintér, et al., Determination of
613 uv-visible-nir absorption coefficient of graphite bulk using direct and indirect methods, *Appl.*
614 *Phys. A: Mater. Sci. Process.* 123 (10) (2017) 633.
- 615 [73] R. Subramanian, G.L. Kok, D. Baumgardner, A. Clarke, Y. Shinozuka, T.L. Campos, et
616 al., Black carbon over mexico: The effect of atmospheric transport on mixing state, mass
617 absorption cross-section, and bc/co ratios, *Atmos. Chem. Phys.* 10 (1) (2010) 219-237.
- 618 [74] Q.Y. Wang, R.J. Huang, J.J. Cao, X.X. Tie, H.Y. Ni, Y.Q. Zhou, et al., Black carbon
619 aerosol in winter northeastern qinghai-tibetan plateau, china: The source, mixing state and
620 optical property, *Atmos. Chem. Phys.* 15 (22) (2015) 13059-13069.

- 621 [75] Y. Wei, L. Ma, T. Cao, Q. Zhang, J. Wu, P.R. Buseck, et al., Light scattering and
622 extinction measurements combined with laser-induced incandescence for the real-time
623 determination of soot mass absorption cross section, *Anal. Chem.* 85 (19) (2013) 9181-9188.
- 624 [76] Y. Zhou, X. Wang, X. Wu, Z. Cong, G. Wu, M. Ji, Quantifying light absorption of iron
625 oxides and carbonaceous aerosol in seasonal snow across northern china, *Atmosphere* 8 (4)
626 (2017) 63.
- 627 [77] S.D. Forestieri, T.M. Helgestad, A. Lambe, L. Renbaum-Wolff, D.A. Lack, P. Massoli,
628 et al., Measurement and modeling of the multi-wavelength optical properties of uncoated flame-
629 generated soot, *Atmos. Chem. Phys. Discuss.* 2018 (2018) 1-39.